GEOCHEMICAL TRANSACTIONS
Geochemical Transactions

RESEARCH ARTICLE Open Access

On the potential for CO_2 mineral storage in continental flood basalts – PHREEQC batch- and 1D diffusion–reaction simulations

Thi Hai Van Pham*, Per Aagaard and Helge Hellevang

Abstract

Continental flood basalts (CFB) are considered as potential CO_2 storage sites because of their high reactivity and abundant divalent metal ions that can potentially trap carbon for geological timescales. Moreover, laterally extensive CFB are found in many place in the world within reasonable distances from major CO_2 point emission sources.

Based on the mineral and glass composition of the Columbia River Basalt (CRB) we estimated the potential of CFB to store CO_2 in secondary carbonates. We simulated the system using kinetic dependent dissolution of primary basalt-minerals (pyroxene, feldspar and glass) and the local equilibrium assumption for secondary phases (weathering products). The simulations were divided into closed-system batch simulations at a constant CO_2 pressure of 100 bar with sensitivity studies of temperature and reactive surface area, an evaluation of the reactivity of H_2O in $scCO_2$, and finally 1D reactive diffusion simulations giving reactivity at CO_2 pressures varying from 0 to 100 bar.

Although the uncertainty in reactive surface area and corresponding reaction rates are large, we have estimated the potential for CO_2 mineral storage and identified factors that control the maximum extent of carbonation. The simulations showed that formation of carbonates from basalt at 40 C may be limited to the formation of siderite and possibly FeMg carbonates. Calcium was largely consumed by zeolite and oxide instead of forming carbonates. At higher temperatures (60 – 100 C), magnesite is suggested to form together with siderite and ankerite. The maximum potential of CO_2 stored as solid carbonates, if CO_2 is supplied to the reactions unlimited, is shown to depend on the availability of pore space as the hydration and carbonation reactions increase the solid volume and clog the pore space. For systems such as in the $scCO_2$ phase with limited amount of water, the total carbonation potential is limited by the amount of water present for hydration of basalt.

Introduction

Underground sequestration of carbon dioxide is a potentially viable greenhouse gas mitigation option as it reduces the release rate of CO_2 to the atmosphere [1]. CO_2 can be trapped subsurface by four storage mechanisms: (1) structural and stratigraphic trapping; (2) residual CO_2 trapping; (3) solubility trapping; and (4) mineral trapping [2]. Mineral trapping has been considered as the safest mechanism in long-term storage of CO_2 [3].

Mineral storage of CO_2 in basaltic rocks is favored over siliciclastic reservoirs both by the higher abundance of divalent metal ions in basalt and the faster reactivity of basaltic glass or crystalline basalt [4]. Moreover, basalts such as the Columbia River flood basalts (CRB) are abundant and in many places close to CO_2 point source emissions [5]. During the last decade several flood basalts around the world have been mapped for the possibility of CO_2 storage, and possible candidates such as CRB in USA and the Deccan traps in India have been identified [4-6].

To be a candidate for CO_2 storage, the flood basalt must have a proper sealing and sufficient injectivity, the latter limited by the available connected pore space. In

* Correspondence: vtpham@geo.uio.no
Department of Geosciences, University of Oslo, Pb. 1047, Blindern, Oslo, Norway

flood basalts, the connected pore space is typically found at zones containing abundant vesicles or in breccias between basalt flows. Because central zones of flood basalts commonly are dense and impermeable without vesicles, and flows are laterally continuous over large areas and commonly stacked vertically for hundreds of meters, flow units can act as seals [5]. The non-porous inner parts of flows may however be penetrated by networks of vertical fractures. These fractures can be open and conductive, or closed by mineralization and non-conductive.

The main objectives of this study were to performe batch- and 1D diffusion–reaction numerical simulations to determine the geochemical potential for secondary carbonate formation and to estimate the volume changes and the possibility of self-sealing following the basalt-CO_2 interactions. The CRB system was used as an example case and our results were compared to earlier reported laboratory experiments and numerical simulations of CO_2-basalt interactions. As CO_2 stored underground will distribute spatially in the reservoir to give a range of reactive conditions, such as the potential of reactions by H_2O dissolved in supercritical CO_2 [7,8] or reactions in the H_2O-rich phase from residually trapped CO_2, we divided the simulations into three systems representing different parts of CO_2 storage: (1) basalt alteration in the H_2O-rich phase at constant CO_2 pressure; (2) basalt alteration in a H_2O saturated CO_2 phase, and (3) reactions at the boundary of the CO_2 plume where CO_2 diffuses into the aquifer from the boundary of the CO2 plume (Figure 1).

Methods

All thermodynamic and kinetic calculations were performed using the geochemical code PHREEQC-2 [9]. This code is capable of simulating complex interactions between dissolved gases, aqueous solutions, and mineral assemblages in batch and 1D advection–diffusion-reaction mode. As the code can only model fully saturated systems, natural systems must be simplified to end-member situations, such as given by constant pressure boundary conditions as may be the case close to underground CO_2 plumes, or the assumption of packages (batches) of water reacting along a reaction path with a homogenous sediment or rock body. Based on these limitations we divided the simulations into three systems representing different parts of CO_2 storage: (1) basalt alteration in the H_2O-rich phase at constant CO_2 pressure; (2) basalt alteration in a H_2O saturated $scCO_2$ phase, and (3) reactions at the boundary of the CO_2 plume where CO_2 diffuses into the aquifer from the boundary of the $scCO_2$ plume (Figure 1). In the second case, we assumed that the CO_2 phase had swept through the systems and dried out residual water, giving only dissolved water in the $scCO_2$ phase. In this case an upper limit of carbonation potential was estimated as reactions were allowed to occur until (nearly) all water was consumed, passing the upper 2 mol/Kgw theoretical limit for the Truesdell-Jones activity model [9].

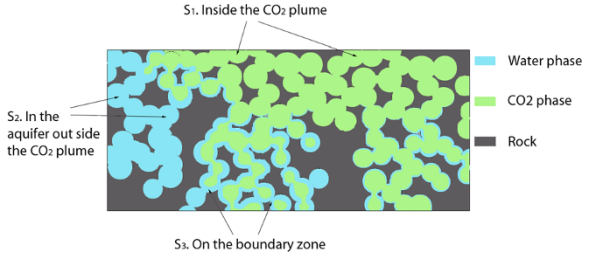

Figure 1 Sketch of possible reaction settings during CO_2 storage in basalt. System 1 (S1) is close to the injector and contains a wet CO_2 (0.5 mole% H_2O at 100 bar and 40 C) with no residual water; system 2 (S2) is fully in the H_2O rich phase with CO_2 diffusing in from the plume boundary; and system 3 (S3) is at the boundary of the CO_2 plume with both sufficient non-wetting CO_2 at a constant CO_2 partial pressure of 100 bar and with sufficient water wetting the mineral surfaces and available for reactions.

The standard state adopted in this study for the thermodynamic calculations was that of unit activity for pure minerals and H_2O at any temperature and pressure. For aqueous species other than H_2O, the standard state was unit activity of the species in a hypothetical 1 molal solution referenced to infinite dilution at any temperature and pressure. For gases, the standard state was for unit fugacity of a hypothetical ideal gas at 1 bar of pressure. All simulations used the llnl.dat database based on the thermo.com. V8.R6.230 dataset prepared at the Lawrence Livermore National Laboratory, with additions of thermodynamic data for those phases not present (see description below).

CO_2 fugacity coefficients were estimated according to the modified Redlich-Kwong (SRK) equation of state [10] and the solubility was adjusted for by a poynting correction term ($exp(v_{CO2}(P_{sat} - P)/RT)$ where v denotes molar volume, P pressure, R the universal gas constant and T absolute temperature) [11]. The density of CO_2 at 40 C and 100 bar was approximated from Bachu and Stewart [12] to be 600 Kg/m^3 and the solubility of water in $scCO_2$ at the same conditions was approximated to 0.5 mole% [13,14]

The simulations were divided into batch simulations of the H_2O rich and CO_2 rich phases respectively, and 1D diffusion of CO_2 in the H_2O rich phase to obtain information on the CO_2-basalt interactions over a continuous range of CO_2 pressures. The latter was solved by PHREEQC using $\partial_t C = D_L \partial_x^2 C + q$, where C denotes molal (mol/Kgw) concentration, q denotes the sink term, subscripts t and x refer to derivatives in time and x-direction respectively, and an efficient diffusion coefficient D_L of 0.45×10^{-9} m^2/s was used for CO_2 [15] and all solutes.

Dissolution rates of minerals in the basaltic rock were calculated according to a kinetic equation taking into account pH and the distance from equilibrium:

$$r_+ = S\left\{k_H exp\left(\frac{-E_{a,H}}{RT}\right)a_H^{n_H} + k_N exp\left(\frac{-E_{a,N}}{RT}\right) + k_{OH} exp\left(\frac{-E_{a,OH}}{RT}\right)a_H^{n_{OH}}\right\}(1-\Omega) \quad (1)$$

where S is the reactive surface area (m^2), k_i are rate constants (moles/m^2s), a_H is the H^+ activity, n is the reaction order with respect to H^+ and OH^-, and Ω is the saturation state given by:

$$\Omega = \exp\left(\frac{\Delta G_r}{RT}\right) \quad (2)$$

Where ΔG_r is the Gibbs free energy of the reaction, R is the gas constant, and T is absolute temperature. Reaction rate constants for crystalline basalt (pyroxenes and plagioclase) were obtained from Palandri and Kharaka [16], and pH dependencies were taken from the same source. The dissolution rate of basaltic glass was calculated according to the expression suggested by Gislason and Oelkers [17]:

$$r_+ = k_+ exp\left(\frac{-E_a}{RT}\right)S\left(\frac{a_{H^+}^3}{a_{Al^{3+}}}\right)^{0.33}(1-\Omega) \quad (3)$$

where k_+ is the far-from-equilibrium dissolution rate coefficient. The saturation state term 1-Ω was approximated to 1 (i.e., rate independent to distance from equilibrium) supported by earlier numerical estimates of glass-CO_2 reactivity suggesting an approximately linear relation between time and reaction progress for basaltic glass [18]. This expression takes into account the effect of pH as well as the effect of the concentration of solutes such as fluoride as they complex with Al^{3+} and reduce the Al^{3+} activity [19]. The specific surface area for basalt (m^2/g) was estimated by:

$$S_{sp} = \frac{\phi}{1-\phi}\frac{A_p}{\bar{\rho}_s V_p} \quad (4)$$

where the ratio A_p/V_p denotes the ratio between pore surface and pore volume (m^{-1}), ϕ is connected porosity, and $\bar{\rho}_s$ (g/m^3) is the density of the basalt solid estimated from the fraction of the individual basalt components. A S_{sp} value of 1.52×10^{-5} m^2/g basalt (= 0.137 m^2/Kg water) was obtained for the CRB using an average basalt solid density of 2.93×10^6 g/m^3 with 10% connected pore space and a A_p/V_p ratio of 400 m^{-1} [5]. The reactive surface area was calculated from the mass of the glass and minerals present according to:

$$S_i = M_i n_i S_{sp} X_r \quad (5)$$

where M and n are molar mass and moles of mineral i, and X_r is the fraction of the total mineral surface that is reactive. As X_r is highly uncertain and is suggested to vary by orders of magnitude [20,21], we used a value of 0.1 for the base case and varied X_r from 1 to 10^{-3}. The use of mass or mass fractions of the individual basalt components to estimate the release rates of elements from the basalt is supported by a recent experimental study which suggests that release rates estimated from the sum of volume fractions of the constituent minerals are within one order of magnitude from measured values [22]. A list of kinetic parameters is given in Table 1. All secondary phases were allowed to form according to the local equilibrium assumption [23].

Changes in solid-phase volumes and porosities ϕ caused by the mineral reactions were calculated according to:

$$\Delta\phi_t = \left(1 - \frac{\sum_i n_{i,t}\bar{v}_i}{V_{total}}\right) - \phi_{t=0} \quad (6)$$

where $\phi_{t=0}$ is the initial porosity, n and $\bar{v}$ are moles and molar volume of mineral i respectively, and V_{total} is the total volume of the system.

The basalt was defined to consist of a mixture of glass and crystalline basalt with mineral and glass fractions chosen based on reported data from CRB [6,24,25]. To represent the crystalline basalt, plagioclase ($Ca_{0.5}Na_{0.5}Al_{1.5}Si_{2.5}O_8$) and the pyroxenes augite ($Ca_{0.7}Fe_{0.6}$ $Mg_{0.7}Si_2O_6$) and pigeonite ($Ca_{1.14}Fe_{0.64}$ $Mg_{0.22}Si_2O_6$) were chosen. The hydrolysis equilibrium constants of these phases were estimated using the PHREEQC program assuming ideal solid solutions of the end-members enstatite, ferrosilite and wollastonite for the pyroxenes, and albite and anorthite for the

Table 1 Kinetic parameters for dissolution of primary minerals based on empirical data given in Palandri and Kharaka [16] and for basaltic glass from [17]

	$k_{\_H}$ (mol/m^2s)	Ea_H kJ/mol	n_H	$k_{\_N}$ (mol/m^2s)	Ea_NkJ/mol	$k_{\_OH}$ (mol/m^2s)	Ea_{OH}kJ/mol	n_{OH}	References
Augite	1.58e-7	78	0.7	1.07e-12	78	-	-		[16]
Pigeonite	1.58e-7	78	0.7	1.07e-12	78	-	-		[16]
Feldspar	1.58e-9	53.5	0.541	3.39e-12	57.4	4.78e-15	59	-0.57	[16]
glass	1e-10	25.5	1	-	-	-	-	-	[17]
Magnetite	2.57e-9	18.6	0.279	1.66e-11	18.6	-	-	-	[16]

plagioclase. Equilibrium constants for the solid solutions for temperatures up to 100 C were estimated with PHREEQC and from these data coefficients *a* to *e* for the PHREEQC built-in analytical expression ($log\ K = a + bT + c/T + dlog_{10}(T) + e/T^2$) were estimated using non-linear regression in MATLAB.

The glass composition ($Ca_{0.015}Fe_{0.095}\ Mg_{0.065}Na_{0.025}\ K_{0.01}Al_{0.105}\ S_{0.003}Si_{0.5}O_{1.35}$) was taken from [6] and modified by adding a small fraction of sulfur which is a common minor constituent of the CR basaltic glass [26].

The secondary mineral assemblage was chosen based on reports on basalt weathering [27-30], with additional carbonates that could potentially form at elevated CO_2 pressures from the release of Fe, Mg and Ca. The ankerite composition chosen for this work was $CaFe_{0.6}\ Mg_{0.4}(CO_3)_2$ which corresponds to a solid solution of 0.6 ankerite ($CaFe(CO_3)_2$) and 0.4 dolomite ($CaMg(CO_3)_2$). Because ankerite ($CaFe_{0.6}\ Mg_{0.4}(CO_3)_2$) was not listed in the thermodynamic database, we estimated values using the same approach as in [31]. The full list of secondary minerals is given in Table 2.

To simulate the CRB-CO_2 interaction we used the average concentrations of solutes reported for the Grand Ronde Formation (Table 3). As supercritical CO_2 ($scCO_2$ at $T > 31.1$ C; $P > 73.9$ bar) is the preferred choice for CO_2 storage, based on higher density compared to gaseous CO_2, we simulated aqueous-phase basalt-CO_2 interaction at a depth of 800 meters at a CO_2 pressure of 100 bar and temperatures of 40 to 100 C. The reactivity of basalt and a H_2O saturated $scCO_2$ phase was simulated using an estimated 0.5 mol% H_2O and a CO_2 density of 600 g/cc giving an initial mass of 0.003 Kg H_2O per 1 liter pore space.

Results

System 1: Basalt alteration in the H_2O-rich phase at constant CO_2 pressure

i) CRB mineral and glass dissolution and formation of secondary minerals

Following the injection of CO_2 into the system, pH immediately decreased from 9.5 to below 4, and thereafter gradually increased to 5.8 at the end of 10000 years (Figure 2a). At the acidic pH secondary phases such as saponite ($Ca_{0.165}Mg_3Al_{0.33}Si_{3.67}O_{10}(OH)_2$), celadonite ($KMgAlSi_4O_{10}(OH)_2$) and zeolite (stilbite) were thermodynamically stable and formed (Figure 2b). Glass dissolved orders of magnitude faster than the crystalline basaltic constituents and more than half dissolved after 10000 years (Figure 2c). The dissolution rate of glass was not increased by the aqueous fluoride as the Al^{3+} activity was fixed by the kaolinite and amorphous silica equilibria. The fluoride therefore only increased the total soluble aluminium. The steady release of Fe from the basalt saturated the water with respect to siderite and a total amount of 10 moles/kgw formed after 10000 years (Figure 2d). Other carbonates, such as ankerite, dolomite, magnesite, and dawsonite did not form as elements such as Mg and Ca was consumed by the non-carbonate secondary phases.

The effect of temperature on the basalt hydration and carbonation was investigated by simulating the system at 60, 80 and 100 C (Figure 3). As for the 40 C simulation we see that basaltic glass dissolves orders of magnitude faster than the crystalline basalt components and the glass is the major source for the secondary phases. The dissolution rates of the basalt components scale exponentially with temperature, and the glass is almost

Table 2 Mineralogy included in the model

	Initial Weight %	Density (g/cm^3)	[2,3]Log K^0
Primary minerals			
[1]Augite (En0.35Fs0.3Wo0.35)	16	3.40	21.00
[1]Pigeonite (En0.57Fs0.32Wo0.11)	3	3.38	21.40
[1]Plagioclase (An50)	35	2.68	14.20
Glass $Ca_{0.015}Fe_{0.095}Mg_{0.065}\ Na_{0.025}K_{0.01}Al_{0.105}\ S_{0.003}Si_{0.5}O_{1.35}$	45	2.92	-99.00
Magnetite	1	5.15	10.47
Secondary minerals			
SiO_2(am)	0	2.62	-2.71
Albite	0	2.62	2.76
Goethite	0	3.80	0.53
Calcite	0	2.71	1.85
Hematite	0	5.30	0.11
Kaolinite	0	2.60	6.81
Smec high Fe-Mg	0	2.70	17.42
Saponite-Mg	0	2.40	26.25
Celadonite	0	3.00	7.46
Stilbite	0	2.15	1.05
Dawnsonite	0	2.42	4.35
Siderite	0	3.96	-0.19
[1]Ankerite ($Ank_{0.6}Do_{0.4}$)	0	3.05	-19.51
Dolomite	0	2.84	4.06
Magnesite	0	3.00	2.29

The mineralogy of the CRB has been described in [25,32] and the weight fraction of pyroxene, feldspar and glass was estimated as average values from the reported data.

[1]Solid solutions. En (enstatite), Fs (ferrosilite), Wo (wollastonite), An (anorthite), Ank (ankerite), Do (dolomite). For details on the calculations of the ankerite solid solution see [31].

[2]Superscript ^{0} denotes Standard state ($T = 298K$, $P = 1$ atm). The equilibrium constant *log K* value is that for the forward dissolution reaction for one mole unit of the mineral.

[3]All thermodynamic data (*log K* and coefficients for the PHREEQC analytical temperature expression) from the llnl.dat PHREEQC database, except for the solid-solutions first estimated in PHREEQC by ideal solid solutions and then added to the PHREEQC database as new solid solution phases.

Table 3 Composition of initial formation water

Elements (totals)	Mol/kgw
Na	1.0×10^{-3}
Ca	6.0×10^{-4}
K	1.0×10^{-4}
Mg	2.0×10^{-5}
Fe	1.2×10^{-6}
Alkalinity (HCO_3^-)	2.0×10^{-3}
Cl	3.0×10^{-4}
S (SO_4^{2-})	1.0×10^{-4}
Si	2.0×10^{-4}
Al	1.0×10^{-6}
Log(O_2)	-10.68
pH	7.5

completely dissolved after 10000 years at 60 C, whereas the time for a complete dissolution takes 4000 and 1500 years at 80 and 100 C respectively (Figure 3a, d, g). The secondary mineral assemblages were largely the same for all temperatures. Stilbite dominated together with amorphous silica (40 and 60 C) and quartz (80 and 100 C) (Figure 3b, e, h). Saponite formed at 40 and 60 C, but not at higher temperatures. Other secondary minerals such as albite, celadonite, and kaolinite formed at all conditions. At 60 C, magnesite and dolomite were still considered to be too slow to form (see [29]) and siderite was the only phase that formed. At 80 and 100 C, magnesite and later ankerite formed together with siderite. Taking zero porosity as the maximum extent of possible reactions we see that the total amount of CO_2 trapped as solid carbonates did not change much with temperature (Figure 4). The reaction rates increased however with temperature and the time needed to reach the maximum potential therefore decreased with temperature (Figure 4).

ii) On the limitation of pore-space for the basalt carbonation

Secondary phases such as stilbite and amorphous silica have lower density than the basalt components and alteration therefore leads to a reduction of pore space. At the presence of CO_2, secondary carbonates further reduce the pore space. For the volume calculations we used expression (6) with the molar volumes listed in Table 2. At 40 C, the starting porosity of 10% is reduced to 0.85% after 10000 years. At the higher temperatures all porosity is lost after 2700, 1200, and 300 years respectively at 60, 80, and 100 C (Figure 5). Taking the extreme of 0% porosity as the limit for the reactions we obtain a maximum carbonation potential (mol CO_2 stored/Kgw) at the different temperatures of 13.5, 29.3, and 28.5 moles for 60, 80, and 100 C (Figure 5). The simulated clogging of the pore space fits well with short-term laboratory percolation experiments on open-system

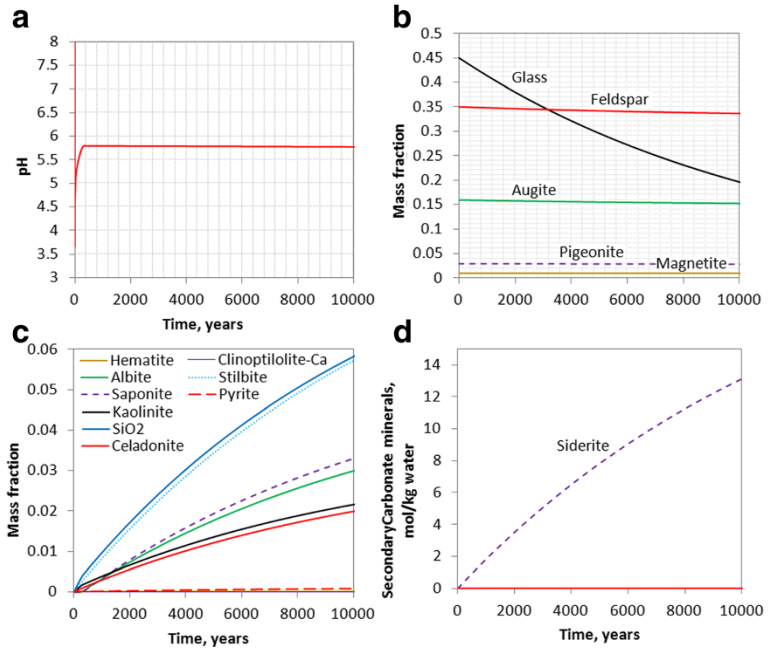

Figure 2 Basalt alteration at 40 C and 100 bar CO_2 pressure over 10000 years. a) pH changes; **b**) mass fractions of basaltic glass and crystalline basalt components; **c**) secondary phases formed; and **d**) moles of secondary carbonates (siderite) formed per kgw.

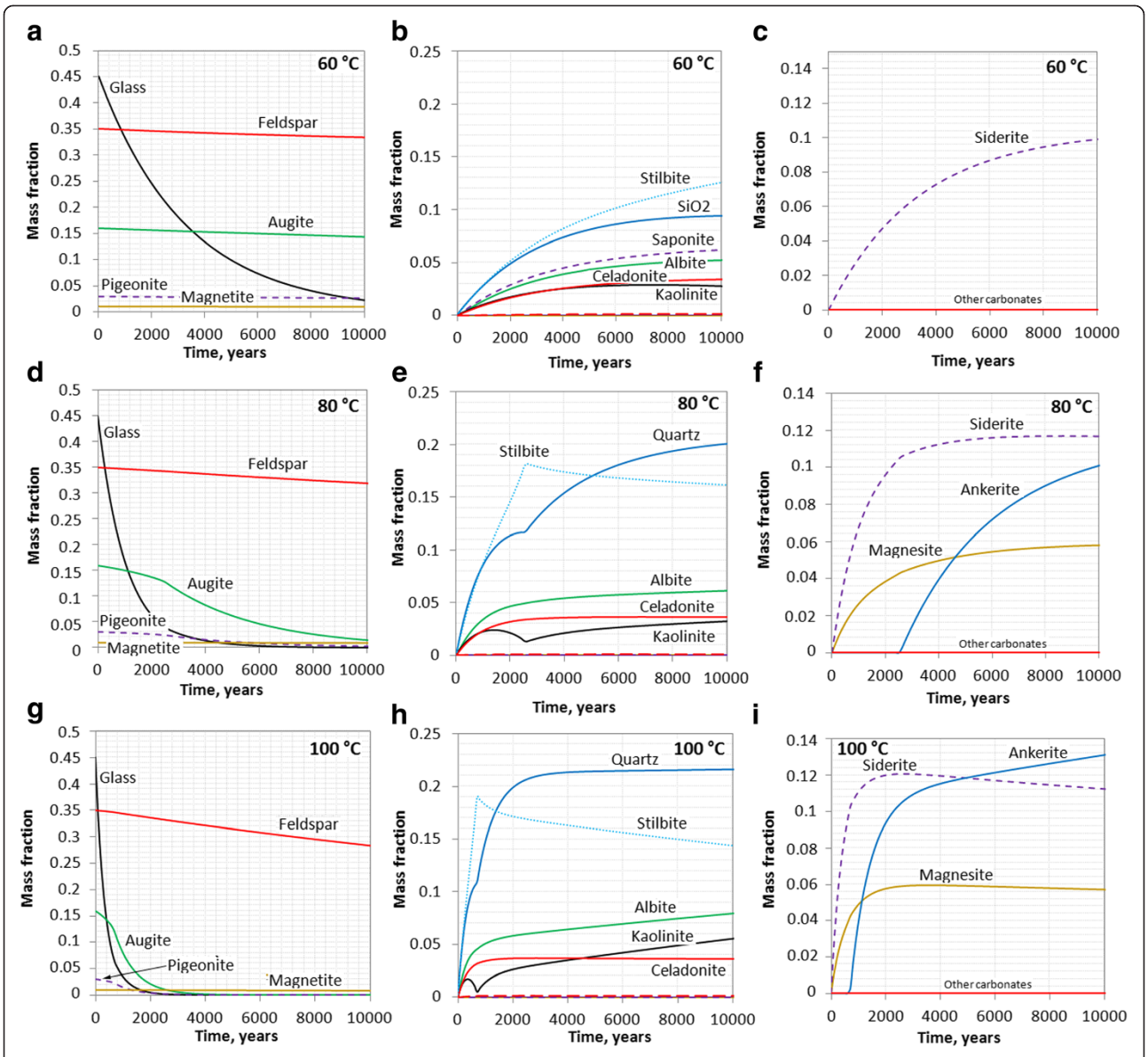

Figure 3 Mass fractions of minerals following basalt alteration at 60, 80, and 100 C over 10000 years: a, **d**, **g**) primary basalt minerals and glass; **b**,**e**, **h**) secondary phases except the carbonates; and **c**, **f**, **j**) carbonates.

basalt-CO_2 alteration which shows loss of porosity and a rapid reduction of permeability during CO_2-basalt interactions (e.g., [33]).

iii) Reduction of pore-space as a function of reactive surface area

As the reactive surface area is a large uncertainty we simulated the changes of porosity over a range of values from a maximum being equal to the estimated physical surface area S_0 (equation (5) with $X_r = 1$) to a three orders of magnitude reduction (Figure 6). The physical conditions of the simulated system was the same as for the base-case at 40 C and a CO_2 pressure of 100 bars. At a reactive surface area that is equal to the estimated S_0 all porosity is lost after approximately 1000 years as stilbite and siderite fills the pore space. If the reactive surface area is reduced by one order of magnitude (i.e. the base case) nearly 1/10 of the original 10% porosity is preserved. Further reductions by one and two orders of magnitude lead to smaller changes and at three orders of magnitude reduction relative to S_0 almost no change is observed (Figure 6).

System 2: The potential for carbonate growth in a H_2O-saturated $scCO_2$ phase

The reaction between H_2O dissolved in $scCO_2$ and basalt was simulated at 100 bar pressure and 40 C. The initial amount of water was 0.003 Kg and no H_2O was

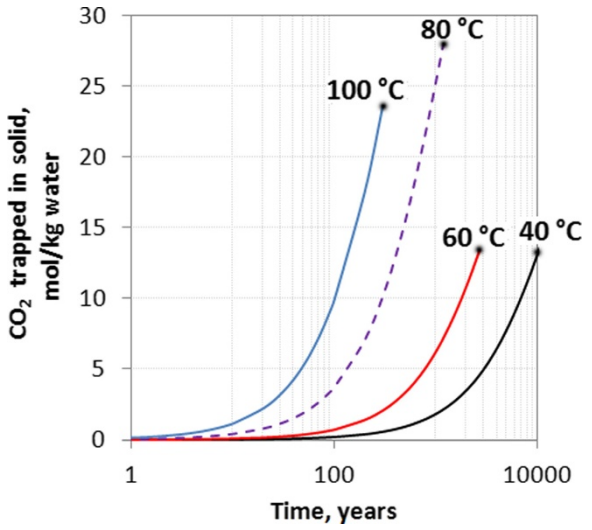

Figure 4 CO_2 trapped in solids for 40 to 100 C simulations at 100 bar CO_2 pressure. A cut-off value is used when all pore space is filled up with the secondary phases (see Figure 5). The simulations suggest that the total amount of secondary carbonates that form is dictated by the available pore space and the thermodynamic stability of secondary phases rather than temperature, whereas carbonate generation rates depend on the exponential increase of basalt dissolution rates with temperature.

allowed to enter the system. This is an ideal end-member case and serves to illustrate the carbonation potential in a volume with limited hydration potential.

As secondary phases such as stilbite formed, water was rapidly consumed and most gone after 45 years

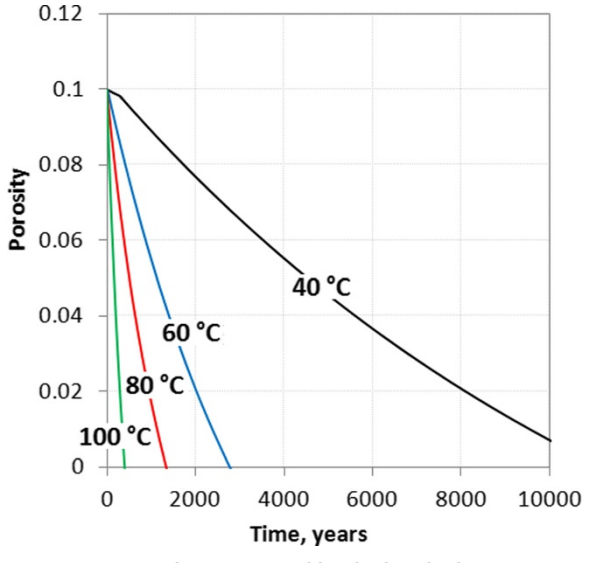

Figure 5 Porosity changes caused by the basalt alteration at 40 to 100 C. Secondary hydrated species and carbonates incorporate the H_2O and CO_2 masses into the solids and clogs the pore space. As reaction rates increase exponentially with temperature, the pore space is filled up faster at the higher temperatures.

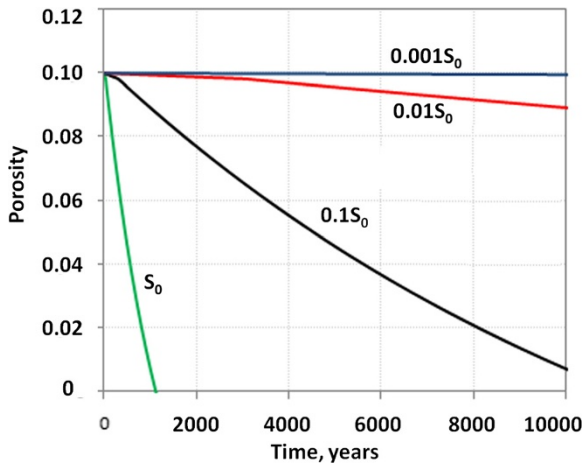

Figure 6 Porosity changes caused by the basalt alteration at 40 C and specific surface areas ranging from S_o (estimated total basalt surface area) down to a three orders of magnitude reduction. The base case specific surface used was S_o/10.

(Figure 7a). At this point stilbite was unstable and supplied water until all water was consumed after approximately 100 years (Figure 7a). Following the basalt hydration, siderite and ankerite formed from the released Ca, Mg, and Fe, with a final total amount of 0.2 moles CO_2 consumed per liter pore space after 100 years (Figure 7b). If H_2O had been allowed to dissolve into the $scCO_2$ phase from residual aqueous phases trapped in the smaller pores, the carbonation potential would have been larger. This process is however, to the knowledge of the authors, not possible to simulate using the PHREEQC code, and was therefore outside the scope of this study.

System 3: 1D diffusion of CO_2 into the CRB aquifer

To see how the basalt reacted under different CO_2 pressures, we defined a 1D diffusion–reaction simulation. This provided us with basalt-CO_2 interactions over a continuous range of CO_2 pressures from the background 1 bar up to the maximum 100 bars. The system corresponds to a stagnant zone presented as a column with one end close to the boundary of the injected CO_2 plume and the other end further away from the plume (Figure 1). The distance reached for the CO_2 into the column is given by the balance between diffusive transport and removal of carbon by secondary carbonate formation. We therefore varied reaction rates from no reaction giving the maximum lengtht of diffusive transport, and up to the base-case rate given by a reaction surface area 1 order of magnitude lower than the estimated physical surface area. Figure 8 shows pH, dissolved CO_2 (mol/Kgw) and amount of secondary carbonate formed in the 1D column. As CO_2 diffuses into the column pH drops to approximately 4 at full

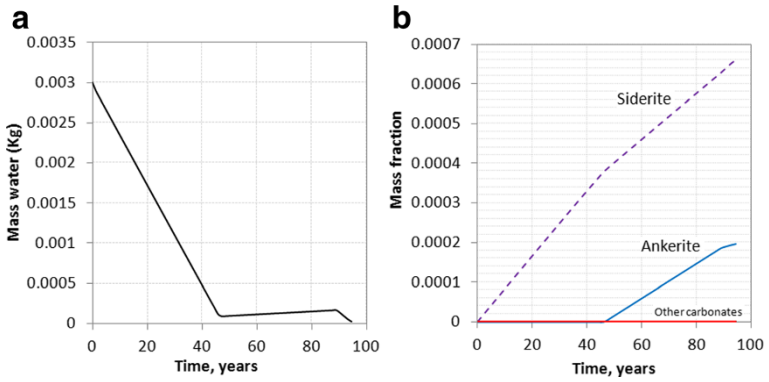

Figure 7 Basalt alteration in the $scCO_2$ rich phase with initial 3 grams of water per liter pore space. A) as zeolites form H_2O is consumed and the water activity is reduced. After approximately 45 years most water is consumed, whereas all is gone before 100 years. **B**) siderite formed the secondary carbonate initially followed by ankerite.

saturation. The depth of diffusion into the 1D column is approximately 40 meters at 1000 years if no carbonate forming reactions occur (Figure 8a). The penetration depth decreased rapidly if reactions were allowed as siderite formed and pulled carbon out of aqueous system (Figure 8b, c). At the highest reaction rate (base-case), CO_2 diffused less than 10 meters into the column as approximately 13 moles/Kgw of siderite formed at the end of the 10000 years simulation (Figure 8d). Siderite formed at greater depth if the reactive surface area was reduced by another order of magnitude, but less formed in total (Figure 8d).

Discussion

Uncertainty on the reactive surface area

The reactive surface area is considered as a major source of uncertainty (e.g., [20,34]) and this leads to corresponding high uncertainties in timing and extent of reactions as dissolution rates have a first order dependence on reactive surface areas. Weathering rates in nature are commonly observed to be 1–3 orders of magnitude lower than in laboratory experiments (e.g., [20,21,34]), and this may in part be explained by differences in reactive and physical (total) surface area between experimental and natural systems. We assumed in this study a base-case reactive surface area 1 order of magnitude lower than the estimated physical surface area for the basalt. A further two orders of magnitude reduction in the reactive surface area, which is within the range of values expected for natural systems, resulted in little basalt alteration and only minor reduction of porosity (see Figure 5). A better understanding of the surface area of porous basalt and the effect of time (aging) on features such as dislocation densities and reactive surface areas are therefore required to understand the potential for CO_2 mineral storage in basaltic rocks.

Uncertainty on the choice of secondary phases used in the model

Growth rate experiments of carbonates such as magnesite and dolomite have shown that the activation energy is high and that growth is negligible at low temperatures (e.g., [35-37]). Dissolution rate studies of siderite suggests that the reaction rate is intermediate between calcite and magnesite [38,39], and growth rate data suggest that siderite may form down to room temperature [40]. Data on ankerite dissolution and growth is to the knowledge of the authors not known. The crystallographic and physical characteristics of ankerite do resemble those of dolomite and siderite, and the chemistry is related to dolomite with the Mg^{2+} substituted by various amounts of Fe^{2+} and Mn^{2+}. If the growth rate is close to the magnesian carbonates such as dolomite and magnesite [41,42], the amount that may form during low-temperature alteration is likely low. In this case, more iron would be available for siderite growth. If on the other hand the growth rate is closer to siderite, we would expect ankerite or other FeMg solid solution carbonates to grow during low-temperature alteration.

One uncertainty related to the local-equilibrium assumption is on the growth retention time for the secondary carbonates. The local-equilibrium assumption predicts growth of the secondary phases as soon as an infinitesimally small supersaturation is reached [23]. The time it takes to nucleate sufficient mass to initiate a significant growth may however be hundreds to thousands of years for some secondary phases [31]. There are no nucleation rate data for siderite and ankerite and the retention time is hence unknown.

Finally, the total potential for secondary carbonate growth may be affected by the amount of magnesium and iron that enters ferromagnesian calcites. As a significant fraction of the metal cations may substitute for calcium (e.g., [43]), a iron-magnesium rich calcite may

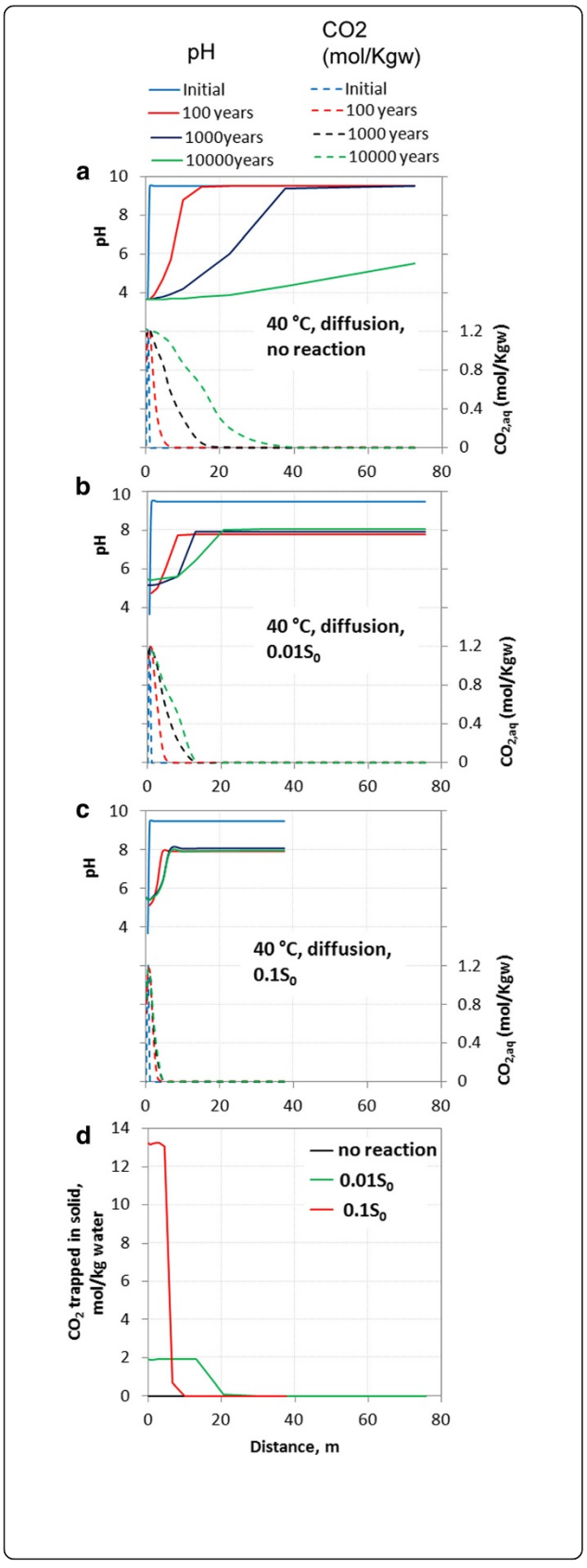

Figure 8 1D reaction–diffusion of CO_2 into permeable basalt. Partial pressure of the inlet boundary was fixed at 100 bar and with a column temperature of 40 C. As consumption of CO_2 by siderite growth affects the depth of CO_2 diffusion, we ran a sensitivity study on reactive surface area going from no reaction **(a)** up to the base case **(c)**. Finally the amount of CO_2 trapped as solid carbonate (siderite) was compared for the base case and reduced reactive surface area **(d)**. We see that the reaction rates strongly constraint the depth of the column affected by the CO_2 diffusion.

potentially form rather than ankerite and thereby reduce the amount of siderite formed.

Comparisons to experiments, numerical simulations and natural analogues of basalt-CO_2 interactions

Our simulations suggest that the potential for carbonate growth is limited to siderite or FeMg carbonates at low temperatures as secondary phases such as zeolites outcompeted the carbonates for calcium. We here compare our simulated results with reported data on CO_2-basalt interactions from laboratory experiments, natural analogues, and other reported numerical simulations.

The reactivity of CRB and other continental flood basalts are available from the long-term (months to years) laboratory experiments done by Schaef and coworkers [6,24]. In these experiments basalt samples from USA, India, South Africa, and Canada were reacted with CO_2 at about 100 bars and 60 to 100 C. Reacted samples from these experiments showed generation of Ca-rich carbonates interpreted as calcites with minor siderite and magnesite. In experiments on CRB using mixtures of H_2S and CO_2 at 60 C and 100 bar and run for 181 days, pyrite (FeS_2) formed together with Mg-Fe poor calcite and a Ca-poor Fe-carbonate [6]. Our simulations at the same temperatures show rapid formation of siderite (60 C) or siderite and magnesite at higher temperatures (Figure 3). Our simulations do not predict any calcite growth as the calcium activity is lowered by zeolite formation. Calcite would however form in our models if the zeolites were not allowed to form at local equilibrium, and possibly if a magnesian ferroan (solid solution) calcite was used in the model instead of the pure end-member calcite. Therefore, the apparent difference between our model and the experiment may be caused by our use of the local equilibrium assumption, whereas the zeolites in the laboratory experiments did not form at low temperatures due to slow kinetics. Recent experiments on basalt dissolution support the preferential release of Mg and Fe over Ca at acidic conditions [22], suggesting that the MgFe-carbonates will dominate as secondary carbonates during CO_2 storage in basalt.

Our numerical simulations share some similarities to other works such as by Marini [18] and Gysi [44], but

our model and hence the outcome is different in several aspects. The most comprehensive work done earlier is the numerical simulations done by Marini [18] on the reactivity of crystalline and glassy CFB following CO_2 storage. The initial mineralogy was similar to our study whereas the temperature of 60 C was slightly higher than our base case 40 C. In [18] the CO_2-basalt interactions were stretched to last for more than 280000 years compared to our 10000 years perspective. The main differences between our model and [18] are on the choice of secondary mineral assemblage, and on the focus of limiting factors such as the availability of water for hydration in the present work. The lack of zeolites and hydrous phases other than kaolinite and goethite in [18] made Ca available for secondary carbonates and the total potential for carbonate formation was higher than in our work. Marini allowed dolomite and magnesite to form at 60 C, whereas our simulations only produced siderite at the similar conditions. Moreover, the formation of dawsonite in [18] is still uncertain and possibly limited at high silica activities and with an assemblage of stable NaAl-silicates defined to form [45]. Based on two different approaches, the reactive surface area for basalt was estimated to quite similar values. We estimated a specific surface area of approximately $1.5x10^{-5}$ m^2/g_{basalt} (= 0.14 m^2/Kg water at 10% porosity) based on the A_p/V_p values estimated by [46] and reported in [5], and reduced this value by one order of magnitude to get the reactive surface area. Marini used a geometric model giving a reactive surface area of 0.41 m^2/Kg water. The higher reactive surface area and higher temperature of [18] resulted in faster reactions and more rapid clogging of the pore space (within a few years). Studies of natural basalt systems at similar or higher temperatures may give some insight into how fast pore space is clogged by basalt hydration or carbonation, and this should be used to improve the estimates of reactive surface areas of basalt for future studies.

Another numerical study on low-temperature (25 C, 30 bar CO_2) basaltic glass alteration was presented by Gysi et al. [44]. Again a main difference is on the choice of secondary minerals. Gysi et al. [44] allowed dolomite, magnesite, and Fe-Mg carbonate to form together with calcite and siderite, whereas we did not allow other Mg-Fe carbonates to form than ankerite. As previously stated, the low-temperature formation of dolomite and magnesite is not likely because of the high apparent activation energy and small kinetic coefficients for the growth of Mg-carbonates [35-37]. Other carbonates such as siderite and potentially FeMg-calcites are more likely to form at these low temperatures. The high reactive surface area used in [44] is based on a geometric model for glass fragments, and is hence not directly comparable with the surface area estimated for a vesicle pore space of a solid basalt. Although no inverse modeling was done to estimate the reactive surface area of the basalt in [44], fragmented basaltic rocks such as hyaloclastite breccias are expected to have significantly higher reactive surface areas than porous solid basalts, and they are therefore correspondingly more reactive.

One example of a natural analogue that shed light on CO_2 basalt interactions is the CO_2 charged basalt hosted groundwaters at Hekla, Iceland. Solution aqueous species sampled from natural cold springs and rivers here showed a drop in total inorganic carbon (TIC) that was interpreted to result from considerable formation of secondary carbonate phases such as calcite [47]. Reaction path modeling of the system suggests however that the carbonate formation is associated with high pH in accordance with the low TIC in the sampled waters. This system is therefore different from basalt CO_2 storage projects where higher CO_2 pressures may be maintained over time and the pH is lower. In addition to calcite, dolomite was also suggested as a potential storage host for the low temperature reactions in Hekla [47]. This may however be questionable as long-term laboratory experiments at room temperature have failed to form dolomite even at significant super saturations [48], explained by the high activation energy for dolomite growth [32,41]. Another natural analogue that more closely corresponds to industrial CO_2 storage is the basalt-hosted petroleum reservoir on Nuussuaq, West Greenland. In this system the bulk carbonate formation appears to have occurred as secondary weathering products. Other alteration products such as zeolites and oxides were replaced by dolomite, magnesite, siderite, and calcite at temperatures of 70–120 C [49]. Therefore, taking into account the basalt weathering products and not only primary basalt minerals appears to be vital in estimating the total potential for secondary carbonate formation and the long-term potential for CO_2 storage in basalt systems.

Summary and conclusions

Simulations of closed-system (P_{CO2} = 100 bar, 40 C) and 1D reaction–diffusion (P_{CO2} = 0–100 bar, 40 C) alteration of basalt suggest that the potential of secondary carbonate formation is limited to siderite at low temperatures as divalent metal cations are preferentially consumed by zeolites and oxides. Higher temperatures 60 – 100 C appear to be in favor of secondary carbonate formation, allowing the precipitation of carbonates such as magnesite, siderite and possibly dolomite and other FeMg carbonates (ankerite). Given an unlimited source of CO_2 (fixed CO_2 pressure), the total amount of CO_2 stored as solid carbonates is orders of magnitude higher than the 1–2 mol/Kg water solubility in the formation water (Figure 4). The total amount trapped might

however be reduced if CO_2, H_2O or pore space are limiting factors. The formation of secondary hydrous and carbonate phases increases the volume of solids and the porosity is correspondingly reduced (Figure 5). This together with the immobilization of CO_2 by solid carbonate formation is in favor of safe long-term storage of CO_2 in basaltic aquifers.

Competing interests

We have no competing interests with any organization to publish the manuscript 'On the potential for CO2 mineral storage in continental flood basalts – PHREEQC batch- and 1D diffusion-reaction simulations'.

Authors' contributions

VTH Pham has made substantial contributions to conception and designs the manuscript. Her contributions are to acquisition of data, analysis and interpretation of data. PA did revising and has given final approval of the version to be published. HH involved in drafting the manuscript, writing methodology part and revising of the final version. All authors read and approved the final manuscript.

Acknowledgements

We highly appreciated constructive comments and suggestions from the reviewers. This work has been funded by SSC-Ramore (Subsurface storage of carbon dioxide - risk assessment, monitoring and remediation) project and (partially) by SUCCESS centre for CO_2 storage under grant 193825/S60 from Research Council of Norway (RCN). SUCCESS is a consortium with partners from industry and science, hosted by Christian Michelsen Research as.

Received: 1 June 2011 Accepted: 14 June 2012
Published: 14 June 2012

References

1. Holloway S: **Underground sequestration of carbon dioxide–a viable greenhouse gas mitigation option.** *Energy* 2004, **30:**2318–2333.
2. Bachu S, Bonijoly D, Bradshaw J, Burruss R, Holloway S, Christensen NP, Mathiassen OM: **CO_2 storage capacity estimation: Methodology and gaps.** *Int J Greenhouse Gas Control* 2007, **1:**430–443.
3. IPCC: **IPCC Special Report on Carbon Dioxide Capture and Storage**. In *In Prepared by Working Group III of the Intergovernmental Panel on Climate Change*. Edited by Metz B, Davidson O, Coninck H, Loos M, Meyer L. Cambridge, United Kingdom and New York, NY, USA: Cambridge University Press; 2005:442 pp.
4. Oelkers EH, Gislason SR, Matter J: **Mineral Carbonation of CO2.** *Elements* 2008, **4:**333–337.
5. McGrail BP, Schaef HT, Ho AM, Chien Y-J, Dooley JJ, Davidson CL: **Potential for carbon dioxide sequestration in flood basalts.** *J Geophysical Res-Solid Earth* 2006, **111:**1–13.
6. Schaef HT, McGrail BP, Owen AT: **Carbonate mineralization of volcanic province basalts.** *Int J Greenhouse Gas Control* 2010, **4:**249–261.
7. Schaef HT, Windish CF, McGrail BP, Martin PF, Rosso KM: **Brucite [$Mg(OH)_2$] carbonation in wet supercritical CO_2: An in situ high pressure x-ray diffration study.** *Geochim Cosmochim Acta* 2011, **75:**7458–7471.
8. White MD, McGrail BP, Schaef HT, Hu JZ, Hoyt DW, Felmy AR, Rosso KM, Wurstner SK: **Multiphase sequestration geochemistry: Model for mineral carbonation.** *Energy Procedia* 2011, **4:**5009–5016.
9. Parkhurst DL, Appelo CAJ: *User's guide to PHREEQC (version 2) - a computer program for speciation, reaction-path, 1D-transport, and inverse geochemical calculations*.: U.S. Geological Survey, Water-Resources Investigation Report; 1999:312.
10. Soave G: **Equilibrium constants from a modified Redlich-Kwrong equation of state.** *Chem Eng Sci* 1972, **27:**1197–1203.
11. Hellevang H, Kvamme B: **ACCRETE - Geochemistry solver for CO_2-water-rock interactions.** *Proceedings GHGT 8 conference* 2006, **:**8p.
12. Bachu S, Stewart S: **Geological sequestration of anthropogenic carbon dioxide in the western Canada sedimentary basin: Suitability analysis.** *J Can Pet Technol* 2002, **41:**32–40.
13. Coan CR, King AD: **Solubility of Water in Compressed Carbon Dioxide, Nitrous Oxide, and Ethane - Evidence for Hydration of Carbon Dioxide and Nitrous Oxide in Gas Phase.** *J Am Chem Soc* 1971, **93:**1857–1862.
14. Sabirzyanov AN, Ilìn AP, Akhunov AR, Gumerov FM: **Solubility of water in Supercritical carbon dioxide.** *High Temp* 2002, **40:**203–206.
15. Bahar M, Lui K: *Measurement of the diffusion coefficient of CO_2 in formation water under reservoir conditions: Implication for CO_2 storage, Society of Petroleum Engineers, SPE Asia Pacific Oil and Gas Conference and Exhibition, 20–22 October 2008*. Perth, Australia:; 2008.
16. Palandri JL, Kharaka YK: *A Complilation of Rate Parameters of Water-Mineral Interaction Kinetics for Applicatin to Geochemical Modeling. U.S. Geological survey, Open report.*: ; 2004:1068.
17. Gislason SR, Oelkers EH: **Mechanism, rates, and consequences of basaltic glass dissolution: II. An experimental study of the dissolution rates of basaltic glass as a function of pH and temperature.** *Geochim Cosmochim Acta* 2003, **67:**3817–3832.
18. Marini L: *Chapter 7: Reaction path Modelling of geological CO_2 sequatration*, In *Geological Sequestration of Carbon Dioxide Thermodynamics, Kinetics, and Reaction Path Modeling*.: Dev Geochem; 2006:319–394.
19. Wolff-Boenisch D, Gislason SR, Oelkers EH: **The effect of fluoride on the dissolution rates of natural glasses at pH 4 and 25 degrees C.** *Geochim Cosmochim Acta* 2004, **68:**4571–4582.
20. White AF, Peterson ML: **Role of reactive-surface-area characterization in geochemical kinetic models**. In *In. Chemical Modeling of Aqueous Systems II*. Edited by Melchior D, *et al*. Washington, DC: ACS Symposium Series, ACS; 1990.
21. White AF, Brantley SL: **The effect of time on the weathering of silicate minerals: why do weathering rates differ in the laboratory and field?** *Chem Geol* 2003, **202:**479–506.
22. Gudbrandsson S, Wolff-Boenisch D, Gislason SR, Oelkers EH: **An experimental study of crystalline basalt dissolution from $2 \leq pH \leq 11$ and temperatures from 5 to 75 C.** *Geochim Cosmochim Acta* 2011, **75:**5496–5509.
23. Helgeson HC: **Evaluation of Irreversible Reactions in Geochemical Processes Involving Minerals and Aqueous Solutions .I. Thermodynamic Relations.** *Geochim Cosmochim Acta* 1968, **32:**853–877.
24. Schaef HT, McGrail BP, Owen AT: **Basalt-CO_2-H_2O Interactions and Variability in Carbonate Mineralization Rates.** *Energy Procedia* 2009, **1:**4899–4906.
25. Schaef HT, McGrail BP: **Dissolution of Columbia River Basalt under mildly acidic conditions as a function of temperature: Experimental results relevant to the geological sequestration of carbon dioxide.** *Appl Geochem* 2009, **24:**980–987.
26. Blake S, Self S, Sharma K, Sephton S: **Sulfur release from the Columbia River Basalts and other flood lava eruptions constrained by a model of sulfide saturation.** *Earth Planet Sci Lett* 2010, **299:**328–338.
27. Neuhoff PS, Fridriksson T, Arnorsson S, Bird DK: **Porosity evolution and mineral paragenesis during low-grade metamorphism of basaltic lavas at Teigarhorn, eastern Iceland.** *Am J Sci* 1999, **299:**467–501.
28. Neuhoff PS, Rogers KL, Stannius LS, Bird DK, Pedersen AK: **Regional very low-grade metamorphism of basaltic lavas, Disko-Nuussuaq region, West Greenland.** *Lithos* 2006, **92:**33–54.
29. Stefansson A, Gislason SR, Arnorsson S: **Dissolution of primary minerals in natural waters - II.** *Mineral saturation state. Chem Geol* 2001, **172:**251–276.
30. Reidel SP, Johnson VG, Spane FA: *Natural gas storage in basalt aquifers of the Colombia Basin, Pacific Northwest USA: A guide to site characterization*. H: Report Pacific Northwest National Laboratory; PNNL-13962; 2002.
31. Pham VTH, Lu P, Aagaard P, Zhu C, Hellevang H: **On the potential of CO_2-water-rock interactions for CO_2 storage using a modified kinetic model.** *International Journal of Greenhouse Gas Control* 2011, **5:**1002–1015.
32. Reidel SP: **A lava flow without a source: the cohassett flow and its compositional components, Sentinel Bluffs Member, Columbia River Basalt Group.** *J Geol* 2005, **113:**1–21.
33. Peuble S, Godard M, Gouze P, Luquot L: **CO_2 sequestration in olivine rich basaltic aquifers: a reactive percolation experimental study.** *Geochim Cosmochim Acta* 2009, **73:**A1635.
34. Velbel MA: **Constancy of silicate-mineral weathering-rate ratios between natural and experimental weathering: implications for hydrologic control of differences in absolute rates.** *Chem Geol* 1993, **105:**89–99.
35. Saldi GD, Jordan G, Schott J, Oelkers EH: **Magnesite growth rates as a function of temperature and saturation state.** *Geochim Cosmochim Acta* 2009, **73:**5646–5657.
36. Arvidson RS, Mackenzie FT: **The dolomite problem; control of precipitation kinetics by temperature and saturation state.** *Am J Sci* 1999, **299:**257–288.

37. Arvidson RS, Mackenzie FT: **Tentative kinetic model for dolomite precipitation rate and its application to dolomite distribution.** *Aquat Geochem* 1996, **2:**273–298.
38. Golubev SV, Bébnézeth P, Schott J, Dandurand JL, Castillo A: **Siderite dissolution kinetics in acidic aqueous solutions from 25 to 100 C and 0 to 50 atm pCO_2.** *Chem Geol* 2009, **265:**13–19.
39. Pokrovsky OS, Golubev SV, Schott J, Castillo A: **Calcite, dolomite and magnesite dissolution kinetics in aqueous solutions at acid to circumneutral pH, 25 to 150 C and 1 to 55 atm pCO_2: New constraints on CO_2 sequestration in sedimentary basins.** *Chem Geol* 2009, **265:**20–32.
40. Greenberg J, Tomson M: **Precipitation and dissolution kinetics and equilibria of aqueous ferrous carbonate vs temperature.** *Appl Geochem* 1992, **7:**185–190.
41. Arvidson RS, Mackenzie FT: **Tentative Kinetic Model for Dolomite Precipitation Rate and Its Application to Dolomite Distribution.** *Aquat Geochem* 1997, **2:**273–298.
42. Saldi GD, Jordan G, Schott J, Oelkers EH: **Magnesite growth rates as function of temperature and saturation state: An HAFM study.** *Geochim Cosmochim Acta* 2009, **73:**A1149.
43. Busenberg E, Plummer LN: **Thermodynamics of magnesian calcite solid-solutions at 25 C and 1 atm total pressure.** *Geochim Cosmochim Acta* 1989, **53:**1189–1208.
44. Gysi AP, Stefansson A: **Numerical modelling of CO_2-water-basalt interaction.** *Mineral Mag* 2008, **72:**55–59.
45. Hellevang H, Declercq J, Aagaard P: **Why is dawsonite absent in CO_2 charged reservoirs?** ***Oil & Gas Science and Technology - Re.*** *IFP Energies nouvelles* 2011, **66:**119–135.
46. Saar MO, Manga M: *The relationship between permeability, porosity, and microstructure in vesicular basalts.*: Master Thesis, Univ. of Oregon, Eugene; 1998:91.
47. Flaathen TK, Gislason SR, Oelkers EH, Sveinbjornsdottir AE: **Chemical evolution of the Mt. Hekla, Iceland, groundwaters: a natural analogue for CO_2 sequestration in basaltic rocks.** *Appl Geochem* 2009, **24:**463–474.
48. Land LS: **Failure to precipitate dolomite at 25 degrees C from dilute solution despite 1000-fold oversaturation after 32 years.** *Aquat Geochem* 1998, **4:**361–368.
49. Rogers KL, Neuhoff PS, Pedersen AK, Bird DK: ***CO_2 metasomatism in a basalt-hosted petroleum reservoir, Nuussuaq, West Greenland.*** *Lithos* 2006, **92:**55–82.

doi:10.1186/1467-4866-13-5
Cite this article as: Van Pham *et al.*: On the potential for CO_2 mineral storage in continental flood basalts – PHREEQC batch- and 1D diffusion–reaction simulations. *Geochemical Transactions* 2012 **13**:5.